Stabilization of Polar Nanoregions in Pb-free Ferroelectrics

A. Pramanick,[1,*] W. Dmowski,[2,3] T. Egami,[2,3] A. Setiadi Budisuharto,[1] F. Weyland,[4] N. Novak,[4]
A. D. Christianson,[5] J. M. Borreguero,[6] D. L. Abernathy,[5] and M. R. V. Jørgensen[7,8]

[1]*Department of Materials Science and Engineering, City University of Hong Kong, Kowloon Tong, Hong Kong SAR*
[2]*Shull Wollan Center, Oak Ridge National Laboratory, Oak Ridge, Tennessee 37831, USA*
[3]*Department of Materials Science and Engineering, University of Tennessee, Oak Ridge, Tennessee 37831, USA*
[4]*Institute of Materials Science, Technische Universität Darmstadt, Darmstadt 64287, Germany*
[5]*Neutron Scattering Division, Oak Ridge National Laboratory, Oak Ridge, Tennessee 37831, USA*
[6]*Neutron Data Analysis and Visualization Division, Oak Ridge National Laboratory, Oak Ridge, Tennessee 37831, USA*
[7]*Center for Materials Crystallography, Department of Chemistry and iNANO, Aarhus University, 8000 Aarhus C, Denmark*
[8]*MAX IV Laboratory, Lund University, SE-221 00 Lund, Sweden*

The formation of polar nanoregions through solid-solution additions is known to enhance significantly the functional properties of ferroelectric materials. Despite considerable progress in characterizing the microscopic behavior of polar nanoregions (PNR), understanding their real-space atomic structure and dynamics of their formation remains a considerable challenge. Here, using the method of dynamic pair distribution function, we provide direct insights into the role of solid-solution additions towards the stabilization of polar nanoregions in the Pb-free ferroelectric of $Ba(Zr, Ti)O_3$. It is shown that for an optimum level of substitution of Ti by larger Zr ions, the dynamics of atomic displacements for ferroelectric polarization are slowed sufficiently below THz frequencies, which leads to increased local correlation among dipoles within PNRs. The dynamic pair distribution function technique demonstrates a unique capability to obtain insights into locally correlated atomic dynamics in disordered materials, including new Pb-free ferroelectrics, which is necessary to understand and control their functional properties.

In materials with inhomogeneous atomic displacements, spins, or elastic distortions [1–5], the presence of nanoscale correlations, instead of a truly random structure, often leads to optimal properties. Examples include ferroelectrics [6–9], manganites with colossal magnetoresistance [10], superconductors [2], spin ice [11], and strain glasses [12]. Understanding both the local structure and dynamics within nanoscale correlated regions is necessary in order to design new materials from a fundamental physicochemical perspective. In spite of several theoretical and experimental advancements, gaining atomistic insights into nanoscale inhomogeneity remains a nontrivial undertaking [13–17]. Here, we demonstrate the ability to obtain structural and dynamic insights into polar nanoregions (PNR) for the Pb-free ferroelectric $Ba(Zr, Ti)O_3$ using recent developments in the dynamic pair distribution function (DPDF) technique [18,19].

Ferroelectrics exhibit a spontaneous electrical polarization due to relative displacements of cations and anions. In some ferroelectrics, PNRs form when correlations among energetically degenerate atomic displacements are confined within nanoscale domains [8]. Recently, there has been intense scrutiny about the nature of PNRs due to their presumed role for highly enhanced dielectric and piezo-electric properties [7,20–22]. In traditional Pb-based ferroelectrics, the "static" atomic displacements within PNRs were modeled based on x-ray and neutron diffuse scattering [6,7]. However, later studies found that PNRs are intrinsically dynamic [18,22], but appear "static" when the frequency of fluctuating dipolar moments is within the energy resolution of the experiment. Furthermore, based on inelastic neutron scattering measurement, a slowing down of PNRs was also proposed for Pb-based ferroelectrics due to a localization of atomic vibrational modes [20,22], although there exists debate on this issue [23,24]. Whereas such developments are noteworthy, it remains difficult to determine the energetics of atomic vibrations within PNRs from phonon scattering alone, especially for the highly damped soft transverse optical (TO) modes.

Because of environmental concerns regarding Pb in electronic components, the search for Pb-free ferroelectrics has intensified [25–27]. Indeed, promising enhancements in functional properties are observed for solid solutions of prototypical Pb-free ferroelectrics, such as $BaTiO_3$ and $KNbO_3$ [25,28,29], which are tentatively linked to microscopic disorder in the form of PNRs [30,31]. However, direct characterization of local structure and dynamics of PNRs in such materials is missing. The local structure of Pb-free ferroelectrics could be substantially different from Pb-based ferroelectrics due to differences in atomic

bonding environments: while hybridization between B-site (Ti or Nb) cation and O plays a major role for ferroelectricity in Pb-free ferroelectrics, Pb-O (A-site) hybridization is more significant for Pb-based ferroelectrics [32,33]. Indeed, unlike Pb-based ferroelectrics, disorder in B-site atomic displacement vectors is observed even in the absence of any chemical substitution for $BaTiO_3$ and $KNbO_3$ [21,34–36]. Additional atomic substitutions are proposed to further modify the local correlations among the B-site atomic displacements in these Pb-free ABO_3 ferroelectrics, leading to formation of PNRs [37]. However, exactly how atomic displacements in PNRs are modified by solid-solution additions is not known. For rational design of Pb-free ferroelectrics, it is expected that such knowledge will be crucial. We demonstrate here direct experimental insights into the local structure and dynamics of PNRs in the Pb-free ferroelectric $Ba(Zr_xTi_{1-x})O_3$.

$Ba(Zr_xTi_{1-x})O_3$ has received great interest as an alternative to Pb-based ferroelectrics due to attractive dielectric, piezoelectric, and electrocaloric properties [38,39]. The phase diagram of $Ba(Zr_xTi_{1-x})O_3$ is shown in Fig. 1(a) [40]. The dielectric permittivity for different x are shown in Fig. 1(b). For $Ba(Zr_xTi_{1-x})O_3$, a transition from normal ferroelectric to relaxor behavior is proposed for composition $x = 0.15$–0.2 [39,41]. Interestingly, the maximum in dielectric permittivity is observed for $x = 0.15$, but then drops sharply and asymmetrically for $x = 0.2$ and beyond. Figure 1(c) compares the ferroelectric hysteresis loops for ceramics of compositions $x = 0.10$ and $x = 0.15$. It is observed that both the maximum (P_{max}) and the remnant polarization (P_r) are larger for $x = 0.15$ as compared to $x = 0.10$, although they both exist in the rhombohedral phase at $-50\,°C$. A similar trend is also observed at $30\,°C$. Such behaviors, in addition to other anomalies as described below, betray the effects of local correlations among disordered polarization vectors.

The trends for $1/\varepsilon_r$ are shown in Fig. 1(d). For a ferroelectric with a relatively large double-well potential, the Curie-Weiss behavior $1/\varepsilon_r \sim (T - T_c)$ is expected as indicated by the straight line, where T_c is the Curie temperature. Deviation from the Curie-Weiss behavior indicates stronger effects of local dipole-dipole correlations [42]. If dipoles are purely a result of zero-point quantum fluctuations, one observes a $1/\varepsilon_r \sim (T - T_C)^2$ behavior [43]. At lower temperatures, the composition $x = 0.15$ shows larger deviation from the Curie-Weiss behavior than $x = 0.10$. Also, since the line for $x = 0.15$ is closer to $1/\varepsilon_r \sim (T - T_C)^2$, it shows that local dipolar correlations are more significant. It is noteworthy that the overall dielectric behavior is affected by both local atomic correlations within PNRs as well as orientational correlations among PNRs. Since the orientational correlation among the PNRs is not expected to change significantly for small changes in composition, it is probable that the local atomic correlations are different for the two compositions. This
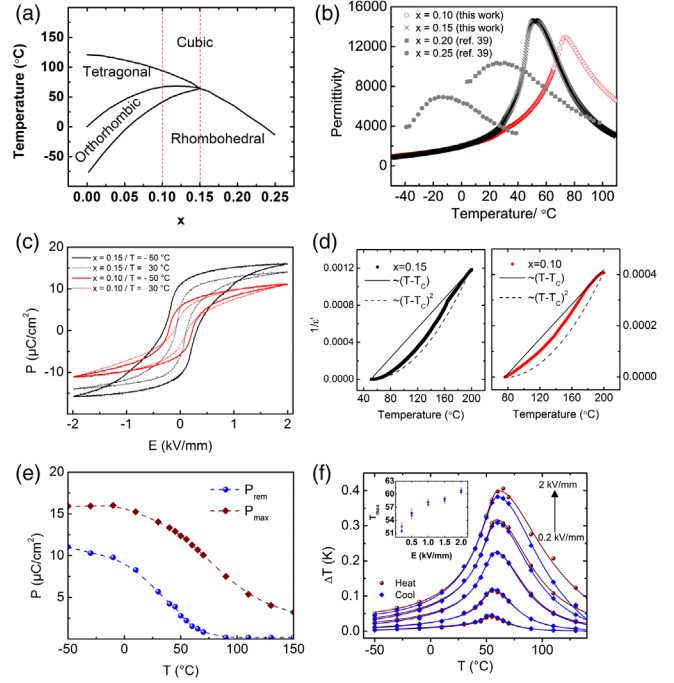

FIG. 1. (a) Phase diagram of $Ba(Zr_xTi_{1-x})O_3$ [39,40]. The compositions used for the current study are shown by dotted lines. (b) Dielectric permittivity ε_r as a function of temperature for different x. (c) Comparison of P-E hysteresis loops for $x = 0.10$ and $x = 0.15$. The decrease in coercive fields at 30 °C is likely due to thermally facilitated initiation of domain-wall motion (d) $1/\varepsilon_r$ for $x = 0.15$ and $x = 0.10$; the scales for the plots are normalized for comparison. The curves are compared to expected behavior for the two exponents. (e) P_r and P_{max} for $x = 0.15$ display nonzero values above T_C. (f) Change in temperature ΔT due to electrocaloric effect for $x = 0.15$. The temperature of maximum ΔT as a function of the applied electric field is shown in the inset.

aspect is further examined below. At higher temperatures, both compositions are close to the Curie-Weiss behavior, indicating the reduced importance of local dipole-dipole correlations.

Evidence of local dipolar correlations can also be observed from temperature-dependent polarization and electrocaloric properties. As shown in Fig. 1(e), for $x = 0.15$, nonzero values for P_{max} and P_r (see Fig. S2 in the Supplemental Material [44]) are observed beyond $T_C \sim 55\,°C$, which can be attributed to the coalescence of local polarization vectors within PNRs [47]. Recently, $Ba(Zr_xTi_{1-x})O_3$ ceramics were also shown to exhibit the giant electrocaloric effect, or adiabatic temperature change ΔT under electric-field application, which can be used for solid-state cooling technologies [39]. Figure 1(f) shows an intriguing behavior of electrocaloric behavior in this material under moderate electric-field amplitudes. For increasing electric-field amplitudes, along with an increase in ΔT, the maximum point for ΔT increases from $\sim 52\,°C$ at 0.2 to $\sim 62\,°C$ at 2 kV/mm. Normally, for ferroelectrics

with first-order phase transition, maximum ΔT is expected at T_C due to a large change in ferroelectric polarization. However, a shift from T_C for maximum ΔT can occur if strong entropic contribution comes from phenomena associated with PNRs [48].

We used the dynamic pair distribution function (DPDF) to investigate the exact nature of local dipole-dipole correlations within PNRs in $Ba(Zr_xTi_{1-x})O_3$. (For details see Supplemental Material [44]). The DPDF or $G(r, E)$ is a function of pairwise atomic distance r and energy E, which is obtained by Fourier transformation of the normalized total scattering factor $S(Q, E)$ over scattering vector Q [18,19]. It reveals the local atomic distance correlations at different frequencies $\nu = E/h$. For $E = 0$, the Fourier transform of $S(Q, E)$ gives the atomic distances of the time-averaged structure, whereas the Fourier transform of the integrated total scattering factor over energy, $S(Q) = \int S(Q, E)dE$, gives the same-time correlations as in conventional pair distribution function (PDF) obtained, for example, by x-ray scattering [15]. Note that the integrated $S(Q)$ pattern (obtained by integrating over all E) is dominated by elastic scattering and therefore the resulting PDF can appear similar to the time-averaged local structure. For further clarification of this point, a comparison with $G(r)$ obtained from energy-integrated profiles is shown in Fig. S10 in the Supplemental Material [44]. The position of a peak in the PDF indicates the distance between a specific atomic pair, while the peak height corresponds to the probability of finding such an atomic pair at this distance. The peak intensities are higher for greater correlations among atomic positions. $G(r, E)$, additionally, provides information on the local structure as a function of frequency or timescales for atomic motions and, therefore, informs us about atomic dynamics within PNRs. The real-space characterization of correlated atomic dynamics is also important for understanding the nature of soft phonon modes, which are usually overdamped and can be localized.

Figure 2(a) shows $G(r, E)$ for $Ba(Zr_xTi_{1-x})O_3$ for $E = 0$ or the time-averaged local structure at $T = 63\,°C$. The peaks for Ti(Zr)-O and Ba-Ti(Zr) indicate off centering of the B atoms. Here, the peak for the Ba-Ti/Ba-Zr bond distance forms a shoulder next to the peak for the same-element correlations [Ba-Ba,Ti(Zr)-Ti(Zr), O-O] at 4 Å. The time-averaged structures for the two compositions are nearly identical, and also matches in terms of peak positions with that reported earlier from neutron and x-ray total scattering for a similar compound [29,47]. Furthermore, the peak widths for the $G(r, E)$ profiles in Fig. 2 are also comparable with that of conventional PDF patterns reported in earlier works [31,49], particularly in the range of $r \sim 3$–4 Å, which is of main interest here. In Fig. 2(b), which shows $G(r, E)$ for $E = 3.4$ meV, we see a clear splitting of the peaks near 4 Å for $x = 0.15$, but not for $x = 0.10$. Also, the Ti(Zr)-O peaks have broadened and
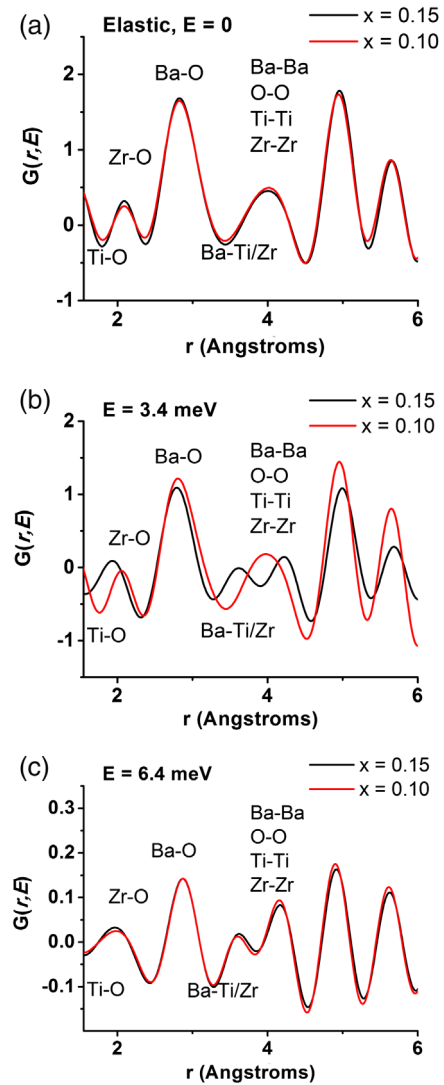

FIG. 2. Comparison of DPDF $G(r, E)$ for $x = 0.15$ and $x = 0.10$ at various energy transfers E, measured at $T = 63\,°C$. The atomic-pair bond distances (r) are marked on the plot. Since the data are obtained using neutron scattering, the Ti-O distance has a negative peak due to the negative scattering length of Ti. The local atomic structural correlations significantly differ for two compositions at the intermediate value of $E = 3.4$ meV.

their centers moved to lower r. In addition, a slight broadening of the peaks at $r \sim 5$ and $r \sim 5.8$ Å can also be observed, which refer to the next-nearest neighbor A-O and the B-O correlations, respectively. These features indicate increased correlation among dynamic off centering of the Ti(Zr) atoms at $E = 3.4$ meV for $x = 0.15$, but not for $x = 0.10$, even though the time-averaged structures for both compositions are identical. Remarkably, $G(r, E)$ for both composition are again near identical for $E = 6.4$ meV [Fig. 2(c)], which indicates that dynamic off-centering of Ti (Zr) atoms are again similarly correlated at higher energies. Indeed, the energy for which peak splitting is observed closely matches with that of zone-center TO modes in

BaTiO$_3$ [50,51]; additionally, the shift in peak positions of ~0.1 Å is consistent with ferroelectric polarization [32,33]. These suggest that the dynamic Ti (Zr) off-centering corresponds to the soft TO vibrational modes. Since both Ti(Zr)-O and Ba-Ti(Zr) bond distances are affected, which additionally indicates that the atomic off centering occurs close to the body diagonal or $\langle 111 \rangle$, consistent with earlier studies [30,34]. While this is hard to deduce from spectroscopic measurements of phonons in Q space, DPDF provides direct information about the specific atomic off centering corresponding to polar vectors in real space.

A 2D plot of DPDF vs r incorporating $G(r, E)$ for all energy-transfer Es at 63 °C [Figs. 3(a), 3(b)] clearly show the differences between the two compositions. The peak splitting at ~4 Å, as described above, occurs at a lower energy E for $x = 0.15$. At the same time, the correlations among dynamic atomic off centerings at lower E are also higher for $x = 0.15$. This is significant, since DPDF measures the atomic pairwise correlations at frequencies $\nu = E/h$. $E = 3.4$ and $E = 6.4$ meV correspond to frequencies of $\nu = 0.8$ and $\nu = 1.6$ THz, respectively.
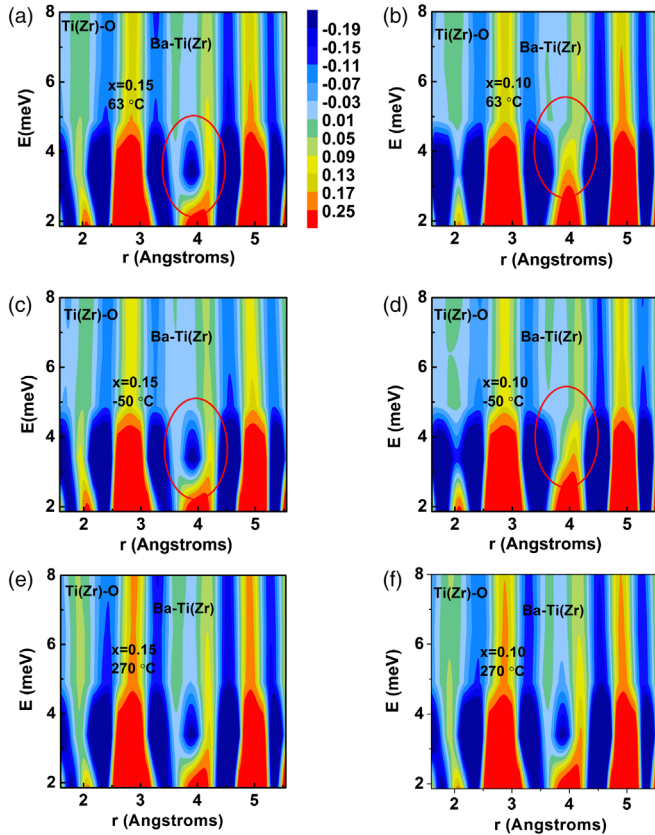

FIG. 3. Composite DPDF patterns $G(r, E)$ for Ba(Zr$_x$Ti$_{1-x}$)O$_3$ for different compositions and temperatures (No smoothing of data has been applied): (a) $x = 0.15$, $T = 63$ °C, (b) $x = 0.10$, $T = 63$ °C, (c) $x = 0.15$, $T = -50$ °C, (d) $x = 0.10$, $T = -50$ °C, (e) $x = 0.15$, $T = 270$ °C, (f) $x = 0.10$, $T = 270$ °C. The DPDF patterns for the two compositions differ at lower temperatures of $T = -50$ °C and 63 °C, but appears similar for $T = 270$ °C.

The fact that the dynamic atomic off centering occurs at lower Es for $x = 0.15$ translates to increased local correlations for such displacements in the time domain. At sub-THz frequencies, the dynamic Ti displacements from TO vibrational modes also approaches that of the hopping motion of Ti ions [35,52], and, therefore, their resonance contributes to the stabilization of PNRs. This is consistent with the data shown in Fig. 1(c), where at lower temperatures, $1/\varepsilon_r$ shows larger deviation from Curie-Weiss behavior for $x = 0.15$. Therefore, we can infer that higher dielectric permittivity peaks as well as higher P_r and P_{max} for $x = 0.15$, as shown in Figs. 1(b), 1(c), mainly originates from stabilization of PNRs through correlated atomic displacements below the THz limit. Stabilization of the PNR dynamics also induces ferroelectric-to-relaxor transition near composition $x = 0.15$, which is responsible for their large electrocaloric properties [39]. Our results support earlier propositions that when correlated atomic vibrations within PNRs slow down below the THz limit, they can significantly enhance macroscopic dielectric and ferroelectric properties [53,54]. This demonstrates the critical role of the solid-solution additive Zr towards enhanced functional properties in Ba(Zr$_x$Ti$_{1-x}$)O$_3$.

Below we explore reasons for increased correlations among dynamic atomic off centering for specific compositions, in this case $x = 0.15$. At $T = 63$ °C, $x = 0.15$ is close to the triple point, where four phases coexist [see Fig. 1(a)]. For $x = 0.10$, the same temperature corresponds to coexistence of tetragonal and orthorhombic phases. In order to examine any role of average phase on local atomic displacements, we performed experiments at −50 °C [Figs. 3(c), 3(d)], where both compositions are in the rhombohedral phase. The corresponding $G(r, E)$ patterns at 63 °C and −50 °C are similar. Therefore, we can conclude that the average phase is not the principal factor for different dynamic atomic displacements. However, structural disorder due to thermal activation does play an important role. At $T = 270$ °C, as shown in Figs. 3(e), 3(f), the $G(r, E)$ patterns are similar for both compositions, which indicate similar correlations among dynamic atomic displacements. This is also consistent with the data shown in Fig. 1(d), where $1/\varepsilon_r$ starts to merge with the Curie-Weiss behavior at higher temperatures.

Since the average phase cannot explain the difference in local dynamic atomic correlations, we explore other possible factors. According to the order-disorder model, the disordered $\langle 111 \rangle$ Ti displacements are locally correlated in the form of nanometers long one-dimensional chains [34]. Introduction of a larger cation at the B site, such as Zr instead of Ti, creates local stresses and disturbs the long-range transverse correlations among the one-dimensional chains [37]. From this line of argument, we would expect that the net polarization should get lowered with progressively increasing addition of Zr. Instead, the dielectric permittivity ε_r peaks at an intermediate Zr content [Fig. 1(b)], indicating nontrivial compositional effects. It is known that stress centers, such as those created by

Zr substitution, can alter the level for double-well potential in ferroelectrics [55], and therefore the frequency of polar displacements at these local centers will also decrease. We also note a recent work, which showed using first-principles calculations that the addition of Zr on Ti sites leads to a flattening of the double-well potential [56]. Therefore, when enough of such centers are created, they can start to coalesce, leading to an overall decrease in energy for dynamic atomic displacements and, consequently, stabilization of polar clusters in the form of PNRs. However, when Zr is added in excess, it causes a net negative effect by creating even more disruption for the transverse correlations among 1D chains as well as by flattening or even removal of the double-well potential. This is likely the reason for the abrupt decrease in dielectric permittivity in $Ba(Zr_xTi_{1-x})O_3$ for $x \geq 0.2$.

In summary, we used the DPDF derived from inelastic neutron scattering to obtain direct insights into the atomic structure and dynamics of PNRs in the Pb-free ferroelectric $Ba(Zr_xTi_{1-x})O_3$. The findings establish that the dynamic B-site atomic displacements occur along $\langle 111 \rangle$ and correlations among these off-center displacements are stabilized for optimum substitutions of Ti by larger Zr atoms. The critical role of Zr addition is to lower the energies for off-center atomic displacements, which consequently reduces the frequency of atomic hopping within the PNRs below THz frequencies. It is proposed that future research on Pb-free ferroelectrics should focus on the effects of solid-solution additions on structure as well as dynamics of atomic correlations at the local level. The current methodology can be used to obtain atomistic insights into locally correlated structures in a wide variety of disordered materials and can therefore help design materials from fundamental physicochemical perspectives.

---

*apramani@cityu.edu.hk

[1] D. A. Keen and A. L. Goodwin, The crystallography of correlated disorder, Nature (London) **521**, 303 (2015).

[2] E. Dagotto, Complexity in strongly correlated electronic systems, Science **309**, 257 (2005).

[3] T. Welberry and D. J. Goossens, Diffuse scattering and partial disorder in complex structures, IUCrJ **1**, 550 (2014).

[4] A. Marthinsen, C. Faber, U. Aschauer, N. A. Spaldin, and S. M. Selbach, Coupling and competition between ferroelectricity, magnetism, strain, and oxygen vacancies in $AMnO_3$ perovskites, MRS Commun. **6**, 182 (2016).

[5] E. Fradkin, S. A. Kivelson, and J. M. Tranquada, Theory of intertwined orders in high temperature superconductors, Rev. Mod. Phys. **87**, 457 (2015).

[6] I.-K. Jeong, T. W. Darling, J. K. Lee, Th. Proffen, R. H. Heffner, J. S. Park, K. S. Hong, W. Dmowski, and T. Egami, Direct Observation of the Formation of Polar Nanoregions in Pb(Mg1/3Nb2/3)O3 using Neutron Pair Distribution Analysis, Phys. Rev. Lett. **94**, 147602 (2005).

[7] G. Xu, J. Wen, C. Stock, and P. M. Gehring, Phase instability induced by polar nanoregions in a relaxor ferroelectric system, Nat. Mater. **7**, 562 (2008).

[8] R. A. Cowley, S. N. Gvasaliya, S. G. Lushnikov, B. Roessli, and G. M. Rotaru, Relaxing with relaxors: A review of relaxor ferroelectrics, Adv. Phys. **60**, 229 (2011).

[9] M. Valant, Electrocaloric materials for future solid-state refrigeration technologies, Prog. Mater. Sci. **57**, 980 (2012).

[10] S. J. L. Billinge, Th. Proffen, V. Petkov, J. L. Sarrao, and S. Kycia, Evidence for charge localization in the ferromagnetic phase of $La_{1-x}Ca_xMnO_3$ from high real-space-resolution x-ray diffraction, Phys. Rev. B **62**, 1203 (2000).

[11] S. Mühlbauer, B. Binz, F. Jonietz, C. Pfleiderer, A. Rosch, A. Neubauer, R. Georgii, and P. Böni Skyrmion lattice in a chiral magnet, Science **323**, 915 (2009).

[12] Y. Wang, X. Ren, and K. Otsuka, Shape Memory Effect and Superelasticity in a Strain Glass Alloy, Phys. Rev. Lett. **97**, 225703 (2006).

[13] D. A. Keen, A comparison of various commonly used correlation functions for describing total scattering, J. Appl. Crystallogr. **34**, 172 (2001).

[14] T. R. Welberry, T. R. Heerdegen, D. C. Goldstone, and I. A. Taylor, Diffuse scattering resulting from macromolecular frustration, Acta Crystallogr. Sect. B **67**, 516 (2011).

[15] T. Egami and S. Billinge, *Underneath the Bragg Peaks: Structural Analysis of Complex Materials*, 2nd ed., Pergamon Materials Series (Elsevier, New York, 2012).

[16] R. L. McGreevy, Reverse Monte Carlo modeling, J. Phys. Condens. Matter **19**, 335218 (2007).

[17] T. R. Welberry and T. Weber, One hundred years of diffuse scattering, Crystallography Reviews **22**, 2 (2016).

[18] W. Dmowski, S. B. Vakhrushev, I.-K. Jeong, M. P. Hehlen, F. Trouw, and T. Egami, Local Lattice Dynamics and the Origin of the Relaxor Ferroelectric Behavior, Phys. Rev. Lett. **100**, 137602 (2008).

[19] T. Egami and W. Dmowski, Dynamic pair-density function method for neutron and x-ray inelastic scattering, Z. Kristallogr. **227**, 233 (2012).

[20] M. E. Manley, J. W. Lynn, D. L. Abernathy, E. D. Specht, O. Delaire, A. R. Bishop, R. Sahul, and J. D. Budai, Phonon localization drives polar nanoregions in a relaxor ferroelectric, Nat. Commun. **5**, 3683 (2014), and references therein.

[21] A. Pramanick, M. R. V. Jorgensen, S. O. Diallo, A. D. Christianson, J. A. Fernandez-Baca, C. Hoffmann, X. Wang, S. Lan, and X.-L. Wang, Nanoscale atomic displacements

ordering for enhanced piezoelectric properties in lead-free ABO$_3$ ferroelectrics, Adv. Mater. 27, 4330 (2015).

[22] M. E. Manley, D. L. Abernathy, R. Sahul, D. E. Parshall, J. W. Lynn, A. D. Christianson, P. J. Stonaha, E. D. Specht, and J. D. Budai, Giant electromechanical coupling of relaxor ferroelectrics controlled by polar nanoregion vibrations, Sci. Adv. 2, e1501814 (2016).

[23] P. M. Gehring, D. Parshall, L. Harriger, C. Stock, G. Xu, X. Li, and H. Luo, Correspondence: Phantom phonon localization in relaxors, Nat. Commun. 8, 1935 (2017).

[24] M. E. Manley, D. L. Abernathy, and J. D. Budai, Correspondence: Reply to 'Phantom phonon localization in relaxors', Nat. Commun. 8, 1936 (2017).

[25] Y. Saito, H. Takao, T. Tani, T. Nonoyama, K. Takatori, T. Homma, T. Nagaya, and M. Nakamura, Lead-free piezoelectrics, Nature (London) 432, 84 (2004).

[26] J. Rödel, W. Jo, K. T. P. Seifert, E.-M. Anton, and T. Granzow, Perspective on the development of lead-free piezoceramics, J. Am. Ceram. Soc. 92, 1153 (2009).

[27] J. Rödel, K. G. Webber, R. Dittmer, W. Jo, M. Kimura, and D. Damjanovic, Transferring lead-free piezoelectric ceramics into application, J. Eur. Ceram. Soc. 35, 1659 (2015).

[28] J. Wu, D. Xiao, and J. Zhu, Potassium-sodium niobate lead-free piezoelectric materials; past, present and future of phase boundaries, Chem. Rev. 115, 2559 (2015).

[29] W. Liu and X. Ren, Large Piezoelectric Effect in Pb-Free Ceramics, Phys. Rev. Lett. 103, 257602 (2009).

[30] A. R. Akbarzadeh, S. Prosandeev, E. J. Walter, A. Al-Barakaty, and L. Bellaiche, Finite-Temperature Properties of Ba(Zr, Ti)O$_3$ Relaxors from First Principles, Phys. Rev. Lett. 108, 257601 (2012).

[31] V. Buscaglia, S. Tripathi, V. Petkov, M. Dapiaggi, M. Deluca, A. Gajovic, and Y. Ren, Average and local atomic-scale structure in BaZr$_x$Ti$_{1-x}$O$_3$ (x = 0.10, 0.20, 0.40) ceramics by high-energy x-ray diffraction and Raman spectroscopy, J. Phys. Condens. Matter 26, 065901 (2014).

[32] R. E. Cohen and H. Krakauer, Lattice dynamics and origin of ferroelectricity in BaTiO$_3$: linearized-augmented-plane-wave total-energy calculations, Phys. Rev. B 42, 6416 (1990).

[33] R. E. Cohen, Origin of ferroelectricity in perovskite oxides, Nature (London) 358, 136 (1992).

[34] R. Comes, M. Lambert, and A. Guinier, The chain structure of BaTiO$_3$ and KNbO$_3$, Solid State Commun. 6, 715 (1968).

[35] A. Pramanick, X. P. Wang, C. Hoffmann, S. O. Diallo, M. R. V. Jorgensen, and X.-L. Wang, Microdomain dynamics in single-crystal BaTiO$_3$ during paraelectric-ferroelectric phase transition measured with time-of-flight neutron scattering, Phys. Rev. B 92, 174103 (2015).

[36] K. Tsuda, A. Yasuhara, and M. Tanaka, Two-dimensional mapping of polarizations of rhombohedral nanostructures in the tetragonal phase of BaTiO$_3$ by the combined use of the scanning transmission electron microscopy and convergent-beam electron diffraction methods, Appl. Phys. Lett. 103, 082908 (2013).

[37] Y. Liu, R. L. Withers, B. Nguyen, and K. Elliot, Structurally frustrated polar nanoregions in BaTiO$_3$-based relaxor ferroelectric systems, Appl. Phys. Lett. 91, 152907 (2007).

[38] A. K. Kalyani, A. Senyshyn, and R. Ranjan, Polymorphic phase boundaries and enhanced piezoelectric response in extended composition range in the lead free ferroelectric BaTi$_{1-x}$Zr$_x$O$_3$, J. Appl. Phys. 114, 014102 (2013).

[39] X.-S. Qian, H.-J. Ye, Y.-T. Zhang, H. Gu, X. Li, C. A. Randall, and Q. M. Zhang, Giant electrocaloric response over a broad temperature range in modified BaTiO$_3$ ceramics, Adv. Funct. Mater. 24, 1300 (2014).

[40] B. Jaffe, W. R. Cook, Jr., and H. Jaffe, Piezoelectric Ceramics (Academic London, Great Britain, 1971).

[41] V. V. Shvartsman, J. Zhai, and W. Kleemann, The dielectric relaxation in solid solutions BaTi$_{1-x}$Zr$_x$O$_3$, Ferroelectrics 379, 77 (2009).

[42] D. Fu, M. Itoh, S.-Y. Koshihara, T. Kosugi, and S. Tsuneyuki, Anomalous Phase Diagram of Ferroelectric (Ba,Ca) TiO$_3$ Single Crystals with Giant Electromechanical Response, Phys. Rev. Lett. 100, 227601 (2008).

[43] T. Ishidate, S. Abe, H. Takahashi, and N. Mori, Phase Diagram of BaTiO$_3$, Phys. Rev. Lett. 78, 2397 (1997).

[44] See Supplemental Material at http://link.aps.org/supplemental/10.1103/PhysRevLett.120.207603 for provides information on details of materials synthesis, dielectric and ferroelectric measurements, electrocaloric measurements and analysis of neutron scattering measurements, which includes Refs. [45,46].

[45] O. Arnold et al., Mantid—Data analysis and visualization package for neutron scattering and image μ SR experiments, Nucl. Instrum. Methods Phys. Res., Sect. A 764, 156 (2014).

[46] W. Dmowski, S. O. Diallo, K. Lokshin, G. Ehlers, G. Ferre, J. Boronat, and T. Egami, Observation of dynamic atom-atom correlation in liquid helium in real space, Nat. Commun. 8, 15294 (2017).

[47] L. M. Garten, P. Lam, D. Harris, J.-P. Maria, and S. Troiler-McKinstry, Residual ferroelectricity in barium strontium titanate thin film tunable dielectrics, J. Appl. Phys. 116, 044104 (2014).

[48] F. Le Goupil, A.-K. Axelsson, L. J. Dunne, M. Valant, G. Manos, T. Lukasiewicz, J. Dec, A. Berenov, and N. M. Alford, Anisotropy of the electrocaloric effect in lead-free relaxor ferroelectrics, Adv. Energy Mater. 4, 1301688 (2014).

[49] C. Laulhe, F. Hippert, R. Bellissent, A. Simon, and G. J. Cuello, Local structure in BaTi$_{1-x}$Zr$_x$O$_3$ relaxors from neutron pair distribution function analysis, Phys. Rev. B 79, 064104 (2009).

[50] J. Harada, J. D. Axe, and G. Shirane, Neutron-scattering study of soft modes in cubic BaTiO$_3$, Phys. Rev. B 4, 155 (1971).

[51] A. Pramanick, S. O. Diallo, O. Delaire, S. Calder, A. D. Christianson, X.-L. Wang, and J. A. Fernandez-Baca, Origins of large enhancement in electromechanical coupling for nonpolar directions in ferroelectric BaTiO$_3$, Phys. Rev. B 88, 180101(R) (2013).

[52] J. Hlinka, T. Ostapchuk, D. Nuzhnyy, J. Petzelt, P. Kuzel, C. Kadlec, P. Vanek, I. Ponomareva, and L. Bellaiche, Coexistence of the Phonon and Relaxation Soft Modes in the Terahertz Dielectric Response Of Tetragonal BaTiO$_3$, Phys. Rev. Lett. 101, 167402 (2008).

[53] V. Bovtun, S. Veljko, S. Kamba, J. Petzelt, S. Vakhrushev, Y. Yakymenko, K. Brinkman, and N. Setter, Broad-band dielectric response of PbMg$_{1/3}$Nb$_{2/3}$O$_3$ relaxor ferroelectrics: Single crystals, ceramics and thin films, J. Eur. Ceram. Soc. 26, 2867 (2006).

[54] D. Wang, A. A. Bokov, Z.-G. Ye, J. Hlinka, and L. Bellaiche, Subterahertz dielectric relaxation in lead-free Ba(Zr, Ti)O$_3$ relaxor ferroelectrics, Nat. Commun. **7,** 11014 (2016).

[55] M. Budimir, D. Damjanovic, and N. Setter, Piezoelectric response and free-energy instability in the perovskite crystals BaTiO$_3$PbTiO$_3$, and Pb(Zr, Ti)O$_3$, Phys. Rev. B **73,** 174106 (2006).

[56] S. Y. Liu, Y. Meng, S. Liu, D.-J. Li, Y. Li, Y. Liu, Y. Shen, and S. Wang, Compositional phase diagram and microscopic mechanism of Ba$_{1-x}$Ca$_x$Zr$_y$Ti$_{1-y}$O$_3$ relaxor ferroelectrics, Phys. Chem. Chem. Phys. **19,** 22190 (2017).